J. Synchrotron Rad. (1998). **5**, 890–892

An ultrahigh-vacuum chamber for surface X-ray diffraction

C. L. Nicklin,* J. S. G. Taylor, N. Jones, P. Steadman and C. Norris

Department of Physics and Astronomy, University of Leicester, University Road, Leicester LE1 7RH, UK. E-mail: cln@le.ac.uk

(*Received 4 August 1997; accepted 4 December 1997*)

An ultrahigh-vacuum environmental chamber for surface X-ray diffraction on Station 9.4 at the Synchrotron Radiation Source, Daresbury Laboratory, is described. Film growth can be monitored by simultaneously recording the Auger signal and the X-ray intensity at a particular point in reciprocal space. Such *in situ* measurements are essential for understanding the dynamic processes that occur during adsorption. An example is given in which the specularly reflected X-ray signal is correlated with Auger plots, during growth of Tl on Cu(001). In addition, the diffractometer and chamber combination allow large reconstructions to be investigated as shown by the in-plane structural analysis of the c(4×4) InSb surface. A study of the layer structure of Cr on Ag(001), in which an extended out-of-plane detector assembly was used, is also presented.

Keywords: surfaces; X-ray diffraction; adsorbates; *in situ* growth measurements; scattering.

1. Introduction

Surface X-ray diffraction (SXRD) in which the primary or scattered beam forms a shallow angle with the surface plane, has become an established and powerful technique for identifying the atomic arrangement in low-dimensional films (Robinson & Tweet, 1992). Its strength lies in the weak interaction of the X-rays with the electrons in the sample, allowing multiple-scattering effects to be neglected and a kinematic approximation to be used for data analysis. A high flux of X-rays is required to achieve measurable diffraction signals and, consequently, most experimental arrangements use synchrotron radiation. The large X-ray penetration depth allows studies in a variety of environments, including ultrahigh vacuum (UHV), in air, high-pressure cells and in liquids. UHV conditions allow the study of atomically clean surfaces and enable SXRD to be correlated with other surface science techniques. Several combinations of UHV system and diffractometer have been reported (*e.g.* Feidenhans'l, 1989, and references therein).

2. Equipment

2.1. *Beamline 9.4*

Beamline 9.4 (Norris *et al.*, 1992) receives radiation from a 5 T wiggler at the Synchrotron Radiation Source (SRS). The white beam is focused, using a platinum-coated silicon toroidal mirror, onto a channel-cut Si(111) monochromator. This allows X-rays of a specific wavelength (in the continuous range 0.7–1.8 Å) to be selected. A series of beam stops and four-jaw slits defines the incident beam on the sample. The scattered X-rays pass through two sets of four-jaw slits, which allow independent definition of the active sample area and the angular resolution of the detector.

2.2. *The diffractometer and ultrahigh-vacuum chamber (Fig. 1)*

The diffractometer (Norris *et al.*, 1986/1987) employs a vertical scattering geometry to take advantage of the polarization of the synchrotron beam. It consists of a four-circle arrangement mounted on a large rotary table (α), allowing the circles and chamber to be turned about a vertical axis centred at the sample position. This enables the grazing angle to be set independently and increases the volume of measurable reciprocal space. An out-of-plane assembly acts as a sixth circle (γ) (Taylor *et al.*, 1996) allowing the detector to be moved to a position 15° along an arc centred at the sample (see Fig. 1). Two partially overlapping regions of reciprocal space can then be accessed, extending the data range in the out-of-plane direction by approximately 50%. This increases the precision with which the positions of the atoms can be determined, normal to the surface. The mount is capable of supporting the liquid-nitrogen-cooled detector, which is generally too heavy for conventional diffractometer circles. This solid-state detector has superior energy resolution to that of a scintillation counter, allowing fluorescence and higher-order scattering to be filtered out and providing a low background level.

The UHV environmental chamber is a stainless-steel vessel into which a 0.5 mm-thick beryllium window that extends over 220° of the circumference by 75 mm in width, has been welded. The inner side is protected by a removable Be foil of thickness 0.1 mm, which prevents evaporation onto the main window during sample cleaning and film deposition. The chamber has ports directed radially towards the sample to allow crystal preparation, characterization and laser alignment. The vacuum is maintained by ion and titanium sublimation pumps. A turbo-molecular pump is used for initial pumping down and during outgassing or argon-sputtering procedures. The base pressure of the system is in the low 10^{-11} mbar range.

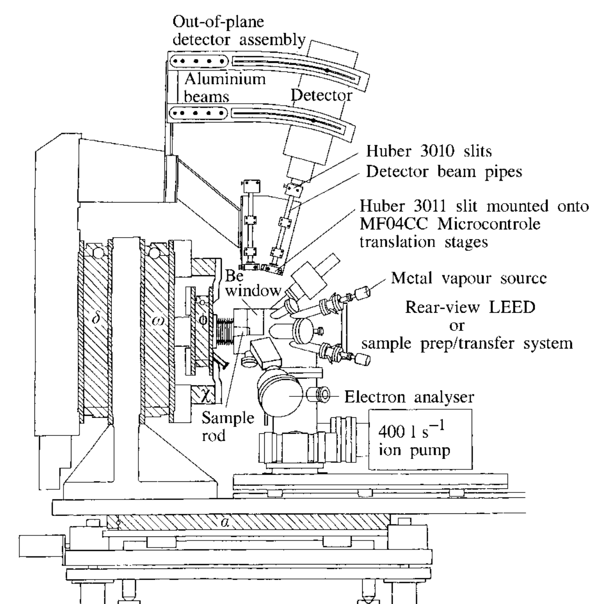

Figure 1
Schematic representation of the UHV environmental chamber shown in position on the diffractometer of Station 9.4. The five conventional axes of the diffractometer are indicated by the shaded regions.

© 1998 International Union of Crystallography
Printed in Great Britain – all rights reserved

2.3. *Rotary seal, manipulators and sample holders*

SXRD requires that the sample and detector are positioned to satisfy a particular diffraction condition for set incident and exit angles (Lohmeier & Vlieg, 1993). The detector is moved using the δ and γ (out-of-plane) axes. The sample is oriented by the ω and φ tables, in addition to the χ arc ($\pm 20^\circ$). The movement is transmitted to the crystal by a two-stage differentially pumped rotatable seal and bellows (Taylor & Norris, 1991). During rotation of the seal, pressure bursts in the chamber are less than 1 $\times$ 10^{-11} mbar.

A liquid-helium-cooled cryostat (Taylor & Norris, 1997) passes through the rotary seal and bellows. It houses a sample holder with integral heater and ensures that the crystal is at the centre of rotation of the diffractometer. All components lie below the sample surface, to avoid high background scatter. The sample is supported by two molybdenum legs, attached to electrical connectors in an alumina base plate. Two additional contacts power a filament located just behind the sample, allowing either radiative or electron bombardment heating.

It is essential that the holder is easily replaced *in situ*, but stable when locked in the manipulator. This is achieved using a centrally positioned rectangular connector in the alumina base plate. It acts as a locator during sample transfer and also fixes the unit in place using a split collet, which is attached to a linear motion feedthrough on the manipulator (Taylor & Norris, 1997). As the collet is retracted, it closes onto the pin; locking it rigid and positioning the sample correctly. The holder also forms a close fit with an outer tube to aid stability.

Cooling is assisted by the collet and outer tube being attached to the cryostat cold finger. The outer support and locator pin are manufactured from copper, ensuring good thermal contact. This arrangement enables the crystal to cool from room temperature to 50 K, in approximately 60 min.

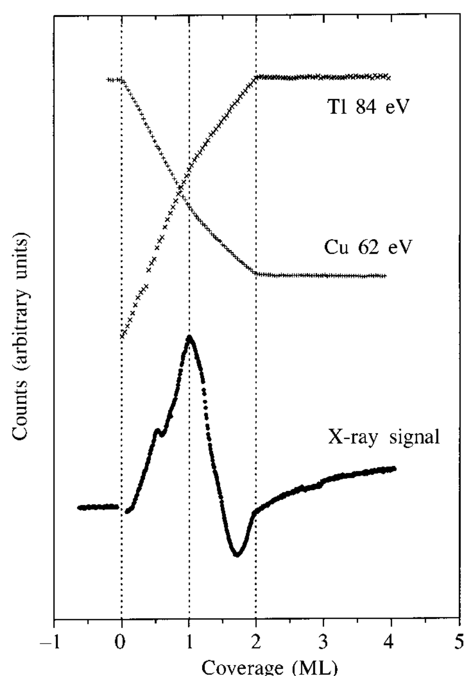

Figure 2
Correlation between the specularly recorded X-ray signal (l = 0.8, wavelength λ = 0.76 Å) and Auger signals of the substrate and adsorbate as a function of deposition time, for Tl grown on Cu(001) at room temperature. Plots have been normalized and offset for clarity.

2.4. *Low-energy-electron-diffraction (LEED) optics and sample-transfer chamber*

Opposite the manipulator, one of two pieces of equipment may be mounted. The first is a rear-view LEED unit supported on a custom-built drive mechanism (Taylor & Norris, 1988). It is readily moved into position over a distance of 230 mm, allowing the surface geometry to be checked. This allows a quick observation of the reconstruction quality and enables correlations between the electron and X-ray diffraction data to be identified.

In experiments requiring sample interchange, a transfer chamber can be mounted. It is a small UHV vessel housing a carousel with six indexed positions, one a hole to allow access into the main chamber and another electrically connected. This allows preliminary outgassing, thus preserving the integrity of the main-chamber vacuum. The remaining positions enable several samples to be stored under vacuum simultaneously. Holders are moved using a magnetically coupled transfer rod.

2.5. *Auger equipment*

Auger electron spectroscopy (AES) measurements are made using a high-energy electron gun and VSW HA-50 electron-energy analyser. The analyser is mounted on retractable bellows beneath the level of the detector, preventing clashes during diffractometer movement (see Fig. 1). This arrangement allows the chemical state of the surface to be determined and the Auger signal of either the substrate or the adsorbate to be monitored during growth, *simultaneously* with X-ray measurements. Correlations between features in the Auger curves and X-ray signal are readily observed. This provides a link between the X-ray measurements and laboratory-based techniques, where Auger equipment is standard.

2.6. *Other equipment: evaporation sources, argon gun, hydrogen source*

In addition to typical surface science equipment (*e.g.* argon sputter gun), up to six compact evaporation sources (Taylor & Newstead, 1987) can be used, enabling complex mixed adsorbate (or multilayer) systems to be studied. An atomic hydrogen source used for cleaning InSb substrates (Jones *et al.*, 1998*a*) can also be mounted on a port pointing at the sample at an angle of 15°.

3. Results

3.1. *In-situ growth measurements*

A powerful insight into the adsorption of ultrathin layers is possible by monitoring the specularly scattered X-ray intensity during growth (Vlieg *et al.*, 1988; Norris, 1993). This reflectivity signal is sensitive to the perpendicular structure of the film and can be calculated using kinematic scattering theory:

$$F_{00l}^{\rm total} = \frac{f_{\rm bulk}\exp\left[-(B_{\rm bulk}q^2/16\pi^2)\right]}{1-\exp\left[-\pi i l-\left(|a_3|/2\mu\right)\right]} + \sum_n \theta_n f_n\left[\exp-\left(B_n q^2/16\pi^2\right)\right]\exp\left[2\pi i l(d_n/|a_3|)\right]$$

where f_j is the atomic scattering factor of the jth atom, μ the penetration depth, B_j the isotropic Debye–Waller parameter and $|a_3|$ the bulk lattice parameter normal to the surface. The first term describes the scattering from the undisturbed bulk. The second term includes contributions from the relaxed topmost layers of the substrate and the adsorbate. Here d_n is the separation of the nth layer from the top of the undisturbed bulk

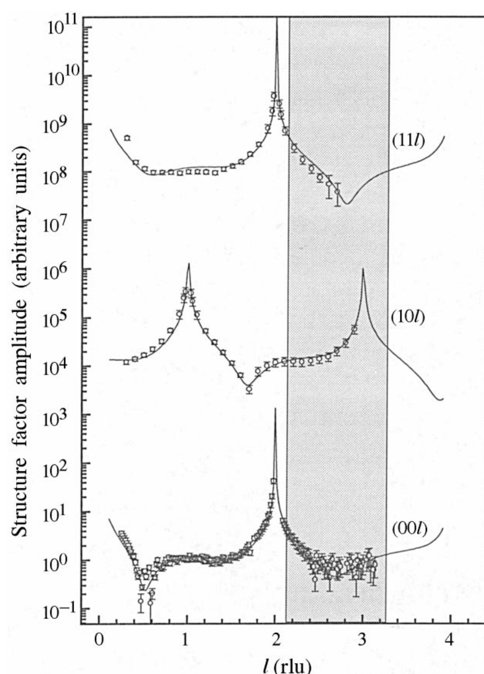

Figure 3
Crystal truncation rods and reflectivity curve for a 2 ML film of Cr grown on a cooled Ag(001) substrate, recorded using X-rays of wavelength 0.9 Å. The shaded region indicates the points that can only be accessed using the out-of-plane detector mount. The fit is outlined in the text. Plots have been offset for clarity.

and θ_n is the fractional coverage, relative to a complete bulk layer. The perpendicular momentum transfer (l) is intimately related to the specular angle. This equation can be used to fit reflectivity data where the intensity is measured as a function of l (constant coverage) and growth curves where the coverage changes (constant l). Heteroepitaxial growth produces intensity fluctuations which depend on the relative scattering strengths of the atoms and the layer separation as well as the coverage.

Fig. 2 shows a growth curve for Tl on Cu(001) (Nicklin *et al.*, 1998). The simultaneous Auger and X-ray measurements at Daresbury allowed data from the European Synchrotron Radiation Facility (ESRF) to be compared with laboratory-based LEED/Auger results. There is a striking correlation between the two measurements; the major peak in the X-ray signal corresponds to a change in gradient of the Auger curves and all three signals level off at twice this peak coverage. These profiles are attributed to the growth of a bilayer followed by island formation. Nicklin *et al.* (1998) confirmed this using reflectivity measurements at different coverages. These data are inconsistent with earlier interpretations, where islanding was suggested to occur after growth of a single Tl layer. The sensitivity of the X-ray signal is indicated by the feature present at 0.5 ML, which is not reflected in the Auger spectra. This is caused by the formation of an ordered surface alloy.

3.2. *In-plane measurements from large-unit-mesh reconstructions*

Surface diffraction from reconstructions with large unit cells has been difficult, due to the amount of data that must be collected. The focusing mirror, fast diffractometer motors and low-noise detector on Station 9.4 have allowed measurements from several large reconstructions, including InSb(001) c(4×4) and c(8×2) surfaces. Jones *et al.* (1998*b*) found that the top layer of the Sb rich c(4×4) reconstruction is characterized by groups of six Sb atoms in a rectangular arrangement. The intra-dimer distance is 3.14 Å for the outer dimers and 2.91 Å for the middle one. These are slightly greater than the nearest-neighbour separation (2.87 Å) in bulk rhombohedral Sb (Wyckoff, 1963). A distance of 4.59 Å separates the dimers, and the model is consistent with sp^3 bonding.

The large amount of data which can be collected indicates that it is feasible to use advanced diffraction analysis, such as maximum-entropy techniques or direct methods, to solve surface structures.

3.3. *Extended out-of-plane data*

The out-of-plane detector assembly has allowed scattering at higher perpendicular momentum transfer (l) to be measured. This is important in the analysis of crystal truncation rod (CTR) and reflectivity data, where the intensity depends on the interference of X-rays from the bulk and surface regions.

Fig. 3 shows (11l) and (10l) CTR data together with the reflectivity (00l) for a 2 ML-thick film of Cr on a cooled Ag(001) substrate (Steadman *et al.*, 1998). The confidence in the fits is increased by the points accessible using the out-of-plane mount. The layer structure is correspondingly better defined. The analysis assumes a roughness model in which the layer coverage is governed by a Fermi–Dirac distribution. It indicates occupancies of 0.99 (interface layer), 0.84 (second layer), 0.16 (third layer) and 0.01 (fourth layer), showing that the growth is almost layer by layer. The fits also reveal an expanded interface layer.

We acknowledge the support of the EPSRC through several grants, most recently GR/J 30707. We would also like to acknowledge our collaboration with the FOM Institute (Amsterdam), Cardiff University and Daresbury Laboratory.

References

Feidenhans'l, R. (1989). *Surf. Sci. Rep.* **10**, 105–188.
Jones, N., Norris, C., Nicklin, C. L., Steadman, P., Taylor, J. S. G., McConville, C. F. & Johnson, A. D. (1998*a*). *Appl. Surf. Sci.* Submitted.
Jones, N., Norris, C., Nicklin, C. L., Steadman, P., Taylor, J. S. G., McConville, C. F. & Johnson, A. D. (1998*b*). *Surf. Sci.* In the press.
Lohmeier, M. & Vlieg, E. (1993). *J. Appl. Cryst.* **26**, 706–716.
Nicklin, C. L., Norris, C., Binns, C., Jones, N., Alvarez, J. & Torrelles, X. (1998). *Surf. Rev. Lett.* In the press.
Norris, C. (1993). *Philos. Trans. R. Soc. London Ser. A*, **344**, 557–566.
Norris, C., Finney, M. S., Clarke, G. F., Baker, G., Moore, P. R. & van Silfhout, R. G. (1992). *Rev. Sci. Instrum.* **63**, 1083–1086.
Norris, C., Taylor, J. S. G., Moore, P. R., Harris, N. W. & Miller, M. (1986/1987). *Daresbury Annual Report*, p. 127. Daresbury Laboratory, Warrington, UK.
Robinson, I. K. & Tweet, D. J. (1992). *Rep. Prog. Phys.* **55**, 599–651.
Steadman, P., Norris, C., Nicklin, C. L., Jones, N. & Taylor, J. S. G. (1998). In preparation.
Taylor, J. S. G. & Newstead, D. A. (1987). *J. Phys. E*, **20**, 1288–1289.
Taylor, J. S. G. & Norris, C. (1988). *J. Phys. E*, **21**, 620–621.
Taylor, J. S. G. & Norris, C. (1991). CMP Technical Memo. Leicester University, UK.
Taylor, J. S. G. & Norris, C. (1997). *Rev. Sci. Instrum.* In the press.
Taylor, J. S. G., Norris, C., Vlieg, E., Lohmeier, M. & Turner, T. S. (1996). *Rev. Sci. Instrum.* **67**(7), 2658–2659.
Vlieg, E., van der Gon, A. W. D., van der Veen, J. F., Macdonald, J. E. & Norris, C. (1988). *Phys. Rev. Lett.* **61**, 2241–2244.
Wyckoff, R. W. G. (1963). *Crystal Structures*, 2nd ed. New York: Interscience.